IBIS/PICsIT Housekeeping data: 5 years monitoring.

INAF/IASF-Bologna
Internal Report n. 505/2008

V. Bianchin

February 12, 2008

With Contributions by
F. Schiavone
G. Di Cocco
L. Foschini
G. Malaguti

Revision History	
Jan 2008	First Version

1 Introduction and Aim

This report describes the monitoring of the IBIS/PICsIT instrument over 5 years of operations, covering the revolutions from number 0036 (29 January 2003) to 0585 (31 July 2007). The starting revolution is number 0036 since previous revolutions were devoted to PV phase (0001 – 0026) and VETO test (0027 – 0035).

Instrument performances stability involves the time evolution study of the following parameters:

- Temperature
- Calibration event rate
- Energy resolution at 511 and 1275 keV
- Gain and Offset
- Background rate, for both single and double pixel events, of Standard Spectral Imaging acquisitions

Parameter trend is inspected on two different time scales: scientific pointing and revolution. More precisely the shortest time scale is given by the on-board integration time, which is a Science Window (~ 2000 s) for counts acquired in Spectral Imaging Mode and ~ 1800 s for calibration events. Temperature, which is recorded every ~ 32 s, is therefore averaged on each ScW.

The local archive at IASF-Bo is briefly described in Bianchin et al. (2008).

IBIS/PICsIT detector monitoring is carried out by means of a set of routines, written in IDL language, which select and visualize housekeeping and processed data. The programme is described in Bianchin et al. (2008).

During the data processing and quality selection a number of anomalies have been recognized, in particular files that have been corrupted during the preprocessing phase. A list of files affected by severe problems that are not recognized by the specific analysis software and that can affect scientific results is given in Tab.8.

2 Hardware Settings - Killed Pixels

Killed pixel history		
Ground	After integration in IBIS	36
	After ground calibration and thermal test	51
In flight	Up to revolution 325	53
	In revolutions 326 – 387	50
	Since revolution 388	52

Table 1: PICsIT killed pixels history

The IBIS/PICsIT instrument is an array of 64 × 64 CsI pixels organized in 8 modules and 16 electronically separated semimodules. Conversely to what happen for the ISGRI layer, when a pixel becomes hot in the PICsIT instrument it is almost permanently switched off and the possible recovery is made by a change in context tables. When noisy pixels are switched off their position is registered in the PICS-PXLP-CFG extension of the *picsit_ctxt_grp* file in the *ic/ibis/cfg* directory (see ISDC/OSA-INTRO (2005) for

data repository structure). At present there are 52 killed pixels (~ 1.3%) and the history of killed and recovered pixels is give in Tab.1.

3 Operational Modes

ST settings		
Period (revolutions)	Time resolution (ms)	Energy Band (keV)
0017 – 0079	62.5	208 – 312
		312 – 676
0080 – 0293	1	156 – 208
		208 – 260
		260 – 364
		364 – 676
0294 – 0440	4	260 – 364
		364 – 676
		676 – 1196
		1196 – 2600
0441–	16	208 – 260
		260 – 312
		312 – 364
		364 – 468
		468 – 572
		572 – 780
		780 – 1196
		1196 – 2600

Table 2: History of settings for the PICsIT Spectral Timing Mode

The IBIS/PICsIT instrument operates in two fundamental modes: Photon-by Photon (PPM) and Standard Mode (SM).

In PPM the complete event list is transmitted to the ground but, due to the high background level in the instrument operational energy range and the on-board telemetry limitations, this mode is activated during Slews or for calibration purpose only.

Scientific observations are acquired in SM, which in turn is the combination of two sub-modes. Spectral

Single Events		Energy	Multiple Events	
bin	channels	keV	bin	channels
1	10-16	203 - 252		
2	17-28	252 - 336		
3	29-40	336 - 448	1	5-12
4	41-56	448 - 672	2	13-28
5	57-82	672 - 1036	3	29-45
6	83-140	1036 - 1848	4	46-74
7	141-198	1848 - 3584	5	75-136
8	199-254	3584 - 6729	6	137-194
		6720 - 9072	7	195-215
		9072 - 13440	8	216-254

Table 3: Standard energy bins for single and multiple events, calculated by the current LUT.

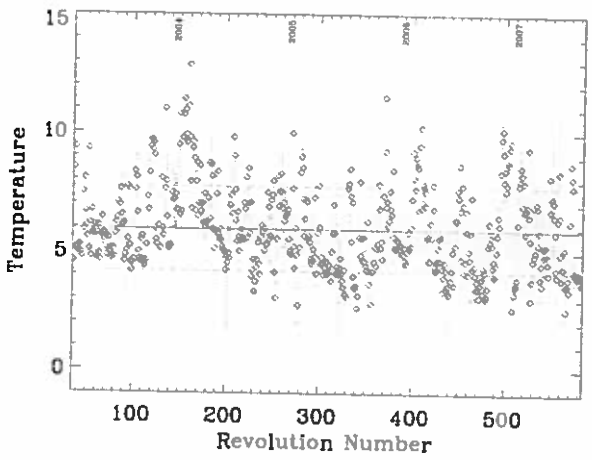

Figure 3: Revolution mean temperature in the revolution range 0036 – 0585. Error bars give the standard deviation. Red and magenta lines are the mean value and the standard deviation on the whole analyzed period.

POINTING_TYPE). The sun aspect associated to each ScW is derived as the mean value of all records in the SUN_ASPECT column corresponding to the POINTING_ID of the ScW at hand and labelled as pointings (P in the POINTING_TYPE column).

From Fig.22-32 temperature and sun aspect seem to have opposite trend, being the former higher for lower angles. This is detailed in Fig.2 where left, central and right panels show respectively, temperature at each sensor, sun aspect and mean detector temperature as a function of the sun aspect. The example refers to the revolution range 0502 – 0513. Note however that the satellite passive structure and payload can shield the radiation flux and smear the correlation. Moreover the sample should be cleaned of the high temperature fluctuations after the instrument switching off during the belt passage. Indeed the dependence is not clear in the T-Sun aspect plane for the overall revolution sample (Fig.33-36).

The evolution of temperature on the overall operation period, from revolution 0036 to 0585, is shown in Fig.3. Each point gives the mean temperature over all acquisition in a given revolution associated with the standard deviation. Note that temperature at sensor level is not corrected for the systematic offset of the thermistors. Red and magenta lines give the mean value and the standard deviation:

$$T = 5.9 \pm 1.8°\mathrm{C} \tag{2}$$

5 Calibration

The on-board calibration unit (OBCU) includes a 0.4μCi (at launch) ^{22}Na radioactive source (half live $\sim$ 2.6 yrs), placed at 220 cm above the instrument. ^{22}Na decays in one photon at 1275 keV (emitted isotropically) and two photons at 511 keV (emitted 180° apart). Calibration events (S5 data) are

S5 channels	S4.0 channels
channel 0	1-48
1	49-50
2	51-52
.....	
31	109-110
32	111-150
33	151-152
34	153-154
.....	
62	209-210
63	211-1024

Table 4: Calibration (S5) and scientific (S4.0) channel relation.

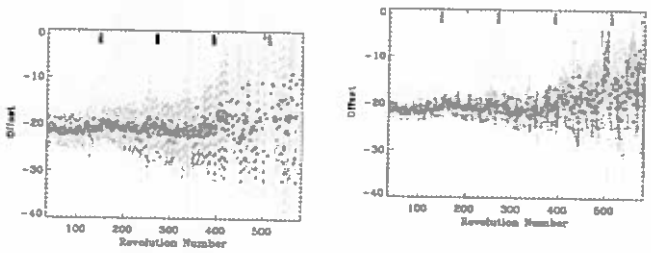

Figure 4: Offset computed for each revolution as the mean value over all calibration files (left panel) and after data integration on each revolution (right panel).

stored in the *picsit_raw_cal_yyyymmddHHMM_xx.fits* files in the *RRRR/rev.001/raw* directory. The PICS-CSI.-CRW extension is a 64 × 64 × 64 array which contains calibration event counts at pixel level, into 64 channels, integrated over the acquisition time that is specified in the INT_TIME parameter in the extension header (typically $\sim$ 1800 *s*). Spectral information is collected in a non linear energy bin scale, having a fine sampling around the two emission lines. The relationship between the 64 S5 channels and the 1024 scientific channels (S4.0) can be derived by the HISTO_CAL field in the *ic/ibis/cfg/pics_hepi_grp_xxxx.fits* and it is summarized in Tab.4. The S5 binning table compresses 48 S4.0 channels in bin 0 and 40 in bin 32 and the other bins are twice the S4.0 bins, according to:

$$ch_{S4.0} = ch_{S5} \times 2 + 48 \quad ch_{S5} \in [1, 32]$$
$$ch_{S4.0} = (ch_{S5} - 32) \times 2 + 150 \quad ch_{S5} \in [33, 64]$$

Gain and Offset are usually defined by the energy/channel relation:

$$E(\mathrm{keV}) = \mathrm{Gain}(\mathrm{keV/ch}) \cdot \mathrm{ch} + \mathrm{Offset}(\mathrm{keV}) \tag{3}$$

and they are derived by the following procedure. The channel spectrum is fitted around each of the 511 and 1275 keV lines to obtain the position of the two peaks. The fitting function is composed by a gaussian for the line and a background term:

$$f(ch) = a + b \cdot ch + c \cdot ch^2 + d \cdot e^{-\frac{ch - ch_0^2}{2\sigma^2}}, \tag{4}$$

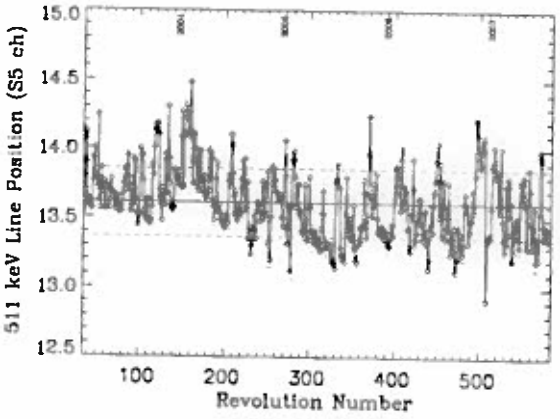

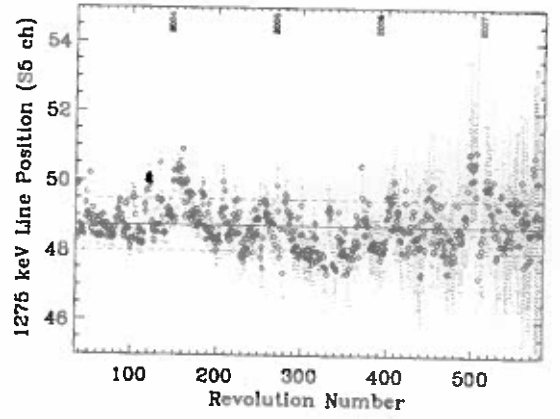

Figure 7: Peak position for 511 and 1275 keV lines computed on integrated spectra for revolutions 0036 – 0585.

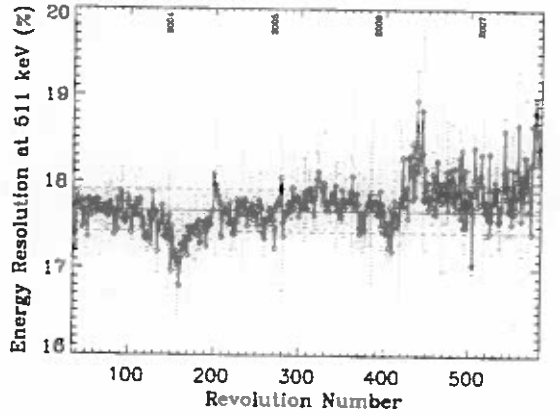

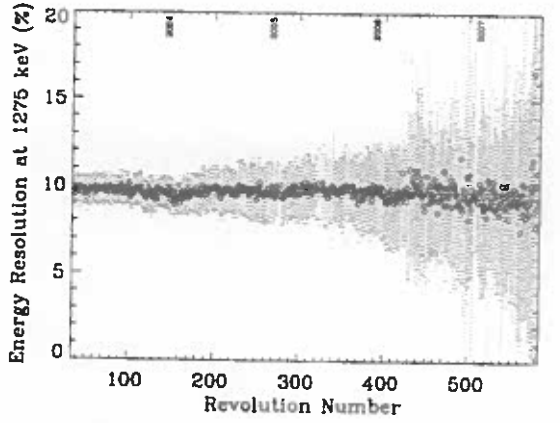

Figure 8: Energy resolution at 511 keV (upper panel) and 1275 keV (lower panel), computed on the revolution integrated spectra, for revolutions 0036 – 0585.

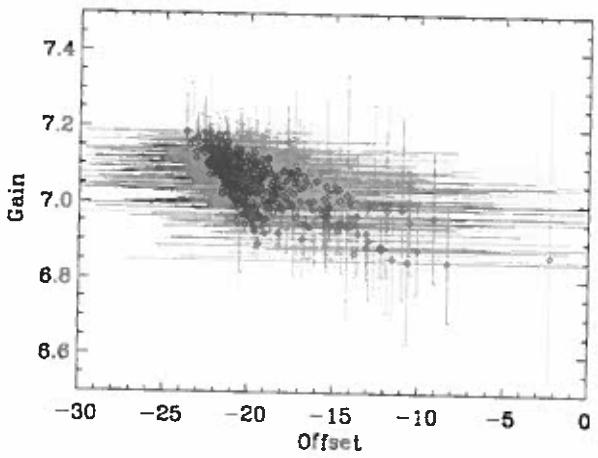

Figure 11: Gain versus offset for parameters at revolution level in the range 0036 – 0585.

the error bars in all the analyzed quantities. This is particularly evident in all plots for quantities compute on short timescale. Parameters at revolution level are better constrained because of longer integration time, however, at the end of the sample, the lack of data and good files does not allow to achieve enough accuracy in the fitting procedure.

5.2 Peak positions

For each calibration file the channel spectrum is fitted in the S5 channel range [4, 23] for the 511 keV line and [35, 61] for the 1275 keV, by the fitting function (4). Fig.6 gives two examples of S5 data maps at the detector plane and channel spectrum together with best fitting function at both lines. Upper left and right panels respectively are for one single file in revolution 0037 and 0578 and lower panels shows integrated spectra over the same revolutions. For technical reasons related to the fit algorithm, the revolution spectrum is normalized to the number of calibration file. In each panel upper maps show integrated counts in the channel intervals [4, 23] and [35, 61] respectively, while the lower map stands for the total counts over the 64 channels. Note the ISGRI spider absorption structure (Bird et al., 2003) in the revolution integrated map at the first line, in the revolution 0037 panel. Comparing spectra and shadowgrams for the two revolutions, it is clear the counts overall deployment, mostly affecting the second line. Moreover maps status for revolution 0578 is because few files are available in this revolution and most have a large number of null/saturated pixels, since for the total spectrum shadowgrams are integrated without data screening.

Line position (parameter *ch0*) at calibration file level is depicted in Fig.41-44 for 511 keV line and Fig.45-

48 for 1275 keV line, grouped in 50 revolutions per plot. By comparing line positions variation with temperature variation, it is noted an increase of both positions with temperature, especially for the 1275keV line.

Line positions computed on the revolution integrated spectra are given in Fig.7, together with the mean value and standard deviation:

$$\begin{aligned} ch0 &= 13.6 \quad \pm 0.2 \quad \text{for line at 511 keV} \\ ch0 &= 48.7 \quad \pm 0.7 \quad \text{for line at 1275 keV} \end{aligned} \tag{5}$$

5.3 Energy Resolution

According to the method described in the previous section, the energy resolution at both lines is derived as the $FWHM/ch0$. In the same respect of the previous analysis, energy resolution at both lines is derived at calibration file level (Fig.49-52 and Fig.53-56 for resolution at 511 and 1275 keV respectively) and at revolution level (Fig.8). The distribution of $\Delta E/E$ computed at file level is shown in Fig.57-60 on groups of 50 revolutions.

The mean value for energy resolution at revolution level computed over the whole sample of revolutions 0036 – 0585 is:

$$\begin{aligned} \Delta E/E &= 17.66 \quad \pm 0.24 \quad \% \quad \text{for line at 511 keV} \\ \Delta E/E &= 9.70 \quad \pm 0.28 \quad \% \quad \text{for line at 1275 keV.} \end{aligned} \tag{6}$$

5.4 Gain & Offset

Gain and Offset are derived (Eq.3) by linearly fitting lines energy and channel position converted in linear (S4.0) scale.

As for all other parameters gain and offset are computed at single calibration file level and for each revolution. Gain for each calibration file is shown in Fig.61-64 for all revolutions in the range 0036 – 0585 grouped in 50 revolutions per plot. Offset is plotted in Fig.65-68 and gain versus offset in Fig.69-72.

Mean gain and offset in each revolution are derived using line position obtained after integrating spectra over each revolution. The evolution on the whole revolution sample is given in Fig.9 and Fig.10. Cyan bars are the error derived from the linear fit procedure. The red and magenta lines give respectively the mean value and the standard deviation on the revolution sample. In Fig.11 the gain-offset dependence is shown, where gain and offset values computed as described above. The progressive worsening in the determination of the parameters is seen on both time scales and this is due to the on-board calibration source degradation. The mean value and the standard deviation for gain and offset on the revolution range 0036 – 0585 are:

$$\begin{aligned} Gain &= 7.06 \pm 0.07 \text{ keV/ch} \\ Offset &= -19.97 \pm 3.59 \text{ keV} \end{aligned}$$

7 Calibration Parameters at Pixel Level

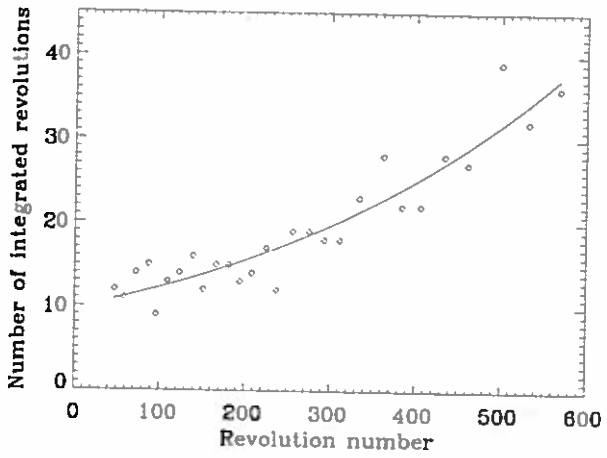

Figure 14: Number of integrated revolutions to obtain reasonable fits.

In order to study the detector disuniformities, line position, energy resolution, gain and offset have been computed at pixel level (see also Di Cocco et al. (2005)). Because of the poor statistic, channel spectra are summed pixel by pixel until parameters are derived with acceptable fit. The integration is performed across multiple revolutions with the minimum increment of counts in one revolution. At each integration step the line fitting of the second peak is attempted in pixel (4, 4). The procedure stops when $\chi^2_r \leq 10$ and then calibration parameters are derived for all pixels. Note that no visual check of the fit quality is available up to date.

The number of summed revolutions increases with time as depicted in Fig.14. Integrated revolution number is superimposed with the theoretical exponential increase, with best fit half live of 2.40 ± 0.06 yr.

Examples of parameters distribution at the beginning and end of the revolution sample are given in Fig 15 and Fig.16. Note the spatial disuniformities modulated at semi-module level, due to semi-module pixel population.

8 Count Rate

Counts are derived from the file *picsit_detector_shadowgram.fits*, containing one extension PICS_DETE_SHD for each energy band for both single and multiples events. In some cases only single or multiple events are available, and the event type is read in the field HIS_TYPE in the Grouping extension. Single and Multiple Events have been analyzed separately according to their multiplicity. Both groups have been restricted to data satisfying the following requirements:

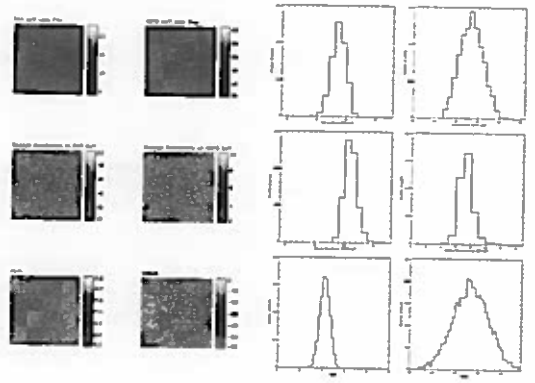

Figure 15: Distribution of line peak, energy resolution, gain and offset computed at pixel level on the detector surface. Single pixel channel spectra have been integrated over 12 revolutions from 0036 to 0047.

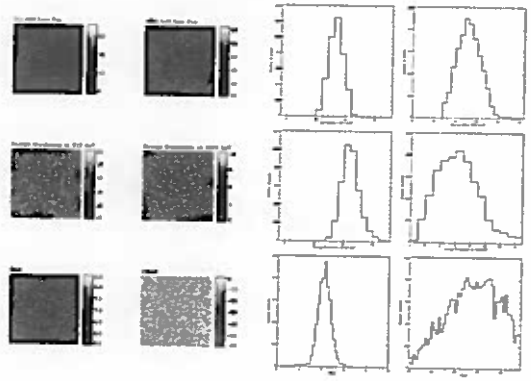

Figure 16: Distribution of line peak, energy resolution, gain and offset computed at pixel level on the detector surface. Single pixel channel spectra have been integrated over 36 revolutions from 0532 to 0567.

- only scientific pointings (ScW) acquired in Standard Mode are selected, by the keyword IBISMODE= 41 in the header of the Grouping extension of the *swg_ibis.fits* file. PPM pointings are just annotated (see Tab.7) and neglected.
- files with more than 1024 null counts pixels have been discarded. This filter neglects files with low exposure and, of greater importance, also recognizes partially downloaded histograms. In principle the pre-processing should mark such files so that they are not included in the scientific analysis. However in few cases the pre-processing fails this step and keywords

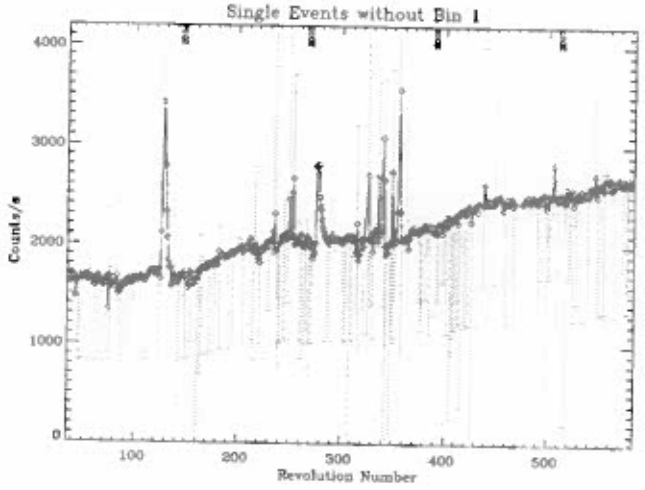

Figure 20: Mean revolution background rate for single events without the first energy bin from revolution 36 to 585.

to the electronic separation of semi-modules, a double event occurring across two semi-modules is not reconstructed in a single energy deposit. This results in a lack of multiple at semi-module borders and corresponding excess of single events (see Malaguti et al. (2002)). This effect is more evident on maps for multiples because of the lower total counts with respect to singles and because a missing double event at given energy is spread in two photons in any lower energy bin.

The maps analysis reveals that few pixels are particularly active in most of energy bands and ScWs and this effect is also visible in the map for total count over revolution (last rows in the panels of Fig.17) where random events are smeared out.

8.2 Short variability (ScW level)

The count rate evolution is inspected at ScW level in the eight standard energy bins for single and multiple events separately. Counts and exposure time for every ScW, energy band and multiplicity are derived from the *picsit_detector_shadowgram.fits* files. The data set includes only acquisitions in standard mode and data have been selected according to filters in Sec.8.

Results are given in Fig.77-86 for single and Fig.88-97 for multiple events. Count rate is plotted as a function of the number of the analyzed ScW on groups of 50 revolutions. Vertical lines divide the analyzed ScWs for different revolutions. Note that only filtered data are plotted among ~ 100 ScWs of each revolution. The list of all pointings contained in each revolution and the number of analyzed ScWs,

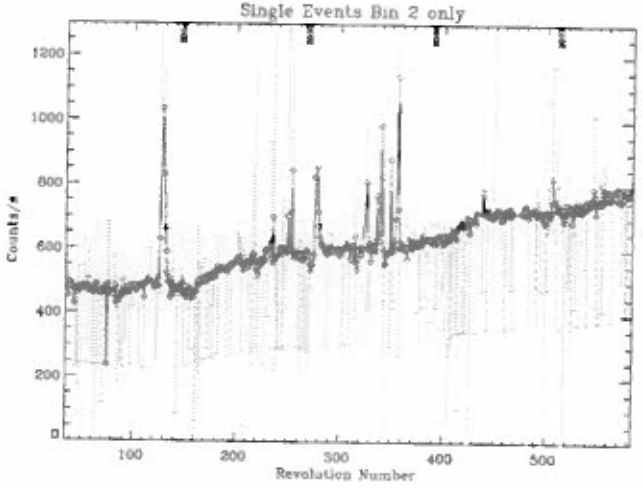

Figure 21: Mean revolution background rate for single events in the second energy band from revolution 36 to 585.

that passed the quality selection, is given in Tab.9-15.

The first energy bin for single events shows the largest variability, due to the cosmic rays induced events mostly affecting the 203 – 252 keV energy band (for more details see Natalucci et al. (2003) and Labanti et al. (2005)).

Several peaks are recognized during the overall analyzed period in all energy bands and for both multiplicity. These are due to high solar events as will be discussed in Sec.8.4.

The lack of files in revolutions 36 – 41 depends on telemetry gaps, change of settings and acquisitions in photon-by-photon during the first calibration phase. The complete list of pointings in PPM is given int Tab.7 Fluctuations of counts are recognized at the beginning of the revolution in the revolution ranges 85 – 92, 142 – 147, 199 – 207, 257 – 266, 317 – 326, 376 – 383, 434 – 441, 492 – 500. For the first four energy bins of singles an increase at the beginning of the revolution corresponds to an opposite trend in the high energy bins and for multiples. This behaviour is simultaneous to large negative excursions of temperature, occurred probably when the IBIS instrument was switched off during the radiation belts passage. The counts variation indicates a temporary change in gain (according with the temperature variation).

At all energy bins both single and multiple events show an overall increase over the operational period. In Tab.5 the percentage of variation of counts from revolution 36 to 585.

Foschini et al., 2007, *IBIS/PICsIT Instrument Specific Software Scientific Validation Report*

Goldwurm A.,David P., Foschini L., Gros A., Laurent P., Sauvageon A., Bird A.J., Lerusse L. and Produit N., 2003, A&A 441, L223

Labanti C., Di Cocco G., Marisaldi M., Foschini L., Produit N., Quadrini E.M., 2005, *Proposal for recovering PICsIT low energy range*

Malaguti G., Di Cocco G., 2003, *PICsIT Spectral Performances: Results from INTEGRAL Payload Ground Calibration & in-flight calibration data*, IN-IM.TES-RP-0052

Malaguti G., Bazzano A., Bird A.J., Di Cocco G., Foschini L., Laurent P., Segreto A., Stephen J. B., Ubertini P., 2003, A&A 441,L173

Malaguti G., Ciocca C., Di Cocco G., Foschini L., Stephen J.B., Valli M., 2002, *The Scientific Characterization of the PICsIT Detector of the IBIS Telescope*, Proceedings of SPIE, 4497, 199

Natalucci L., 2003, *Performances of S7.0 mode preliminary results*, IN-IB-IASF/Rm-RP-0032/03

INTEGRAL Science Data Centre, 2005, *Introduction to the INTEGRAL Data Analysis*

9 Tables

Photon by Photon	
Rev	ScW
0039	000300*-000500*
0040	000200*
0073	00620010, 00650010-00670010
0300	00300010-00500020

Table 7: ScWs acquired in Photon-by-Photon.

PROBLEM	WHERE			PROBLEM	WHERE		
	Rev	ScW	Type		Rev	ScW	Type
difference in exposure and elapsed time	0037	0072	SM	partially downloaded histograms	0307	006	SM
partially downloaded histograms	0047	107	SM		0342	013	M
	0071	067	M		0358	011	M
	0084	002	M		0406	055	M
	0143	075	M		0407	040	S
	0164	111	M		0408	022	M
	0191	054	SM			029	M
	0211	019	SM		0416	096	M
	0217	014	M		0462	008	SM
	0218	035	SM		0491	009	M
	0226	044	SM		0517	032	M
	0239	034	M		0525	056	M
	0268	022	SM		0555	055	SM
					0578	037	SM

Table 8: ScWs affected by severe errors. These files should not be included in the scienific analysis. In the Type column S/M stands for Single/Multiple events.

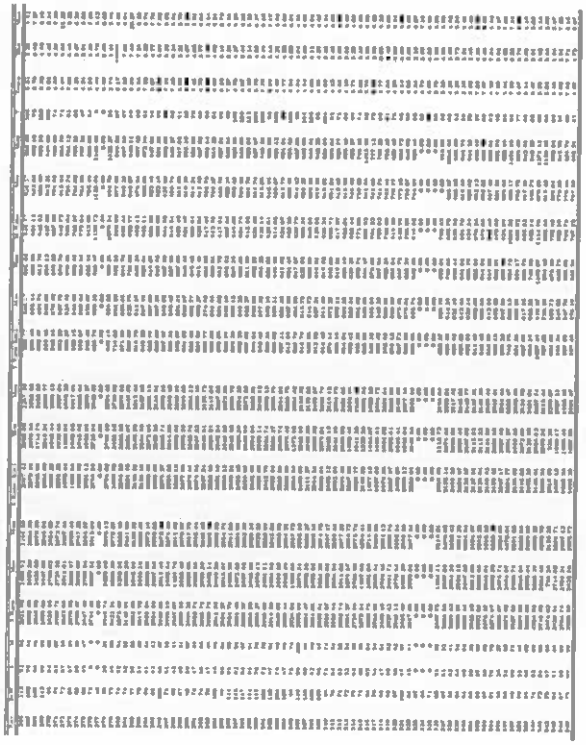

Table 12: ...continue

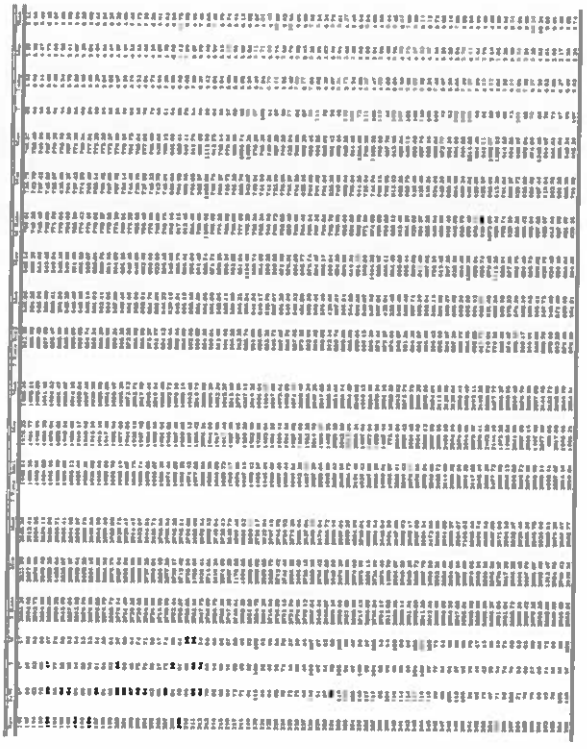

Table 13: ...continue

Table 16: Summary. The table gives for each revolution the total number of calibration files, the number of files that have been included in the sample, the mean value of count rates for SI data, grids effect, position of line and energy resolution at 511 and 1275 keV. Mean parameters are derived from channel spectra integration over each revolution. For each, the maximum and minimum computed at calibration file level is given.

Table 16: ...continue

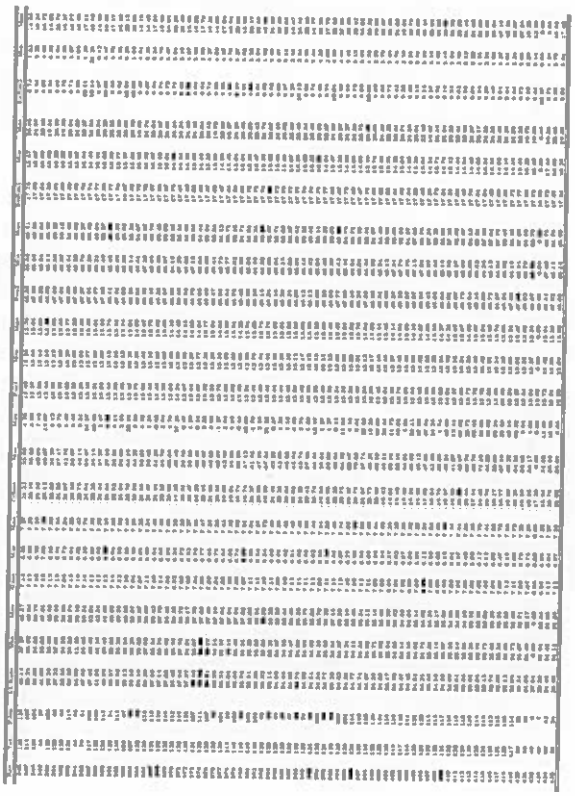

Table 20: ...continue

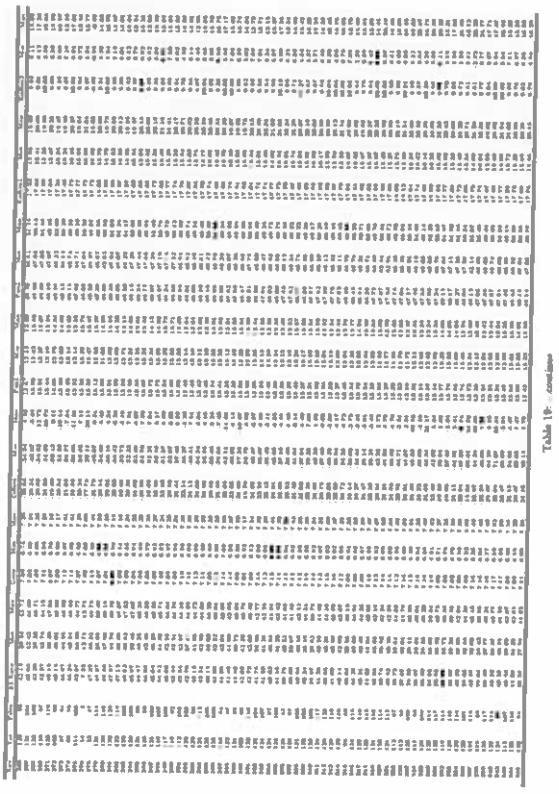

Table 19: ...continue

10 Figures

10.1 Temperature

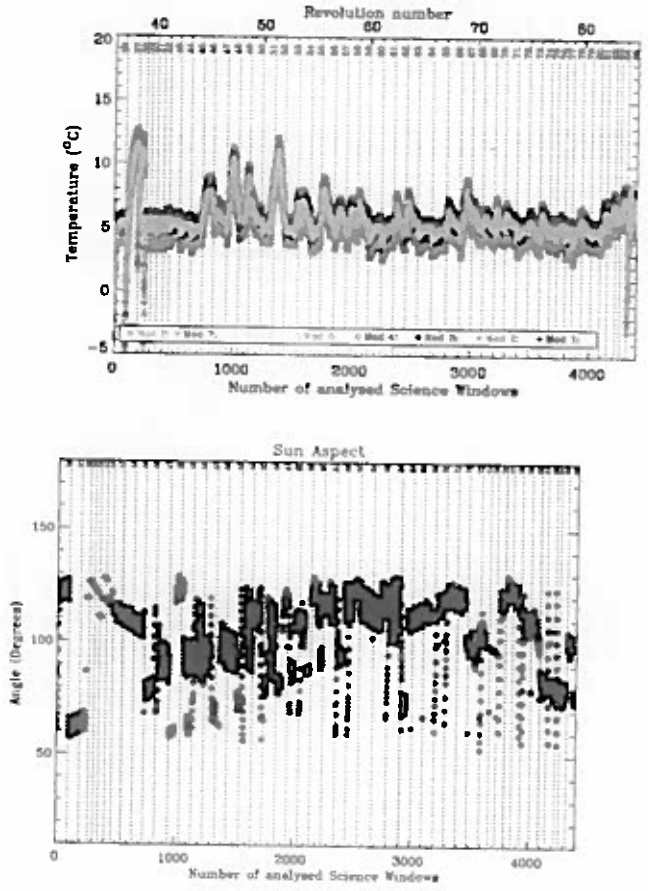

Figure 22: Temperature (upper panel) and sun aspect (lower panel) at ScW level in the revolution range 0036 – 0085

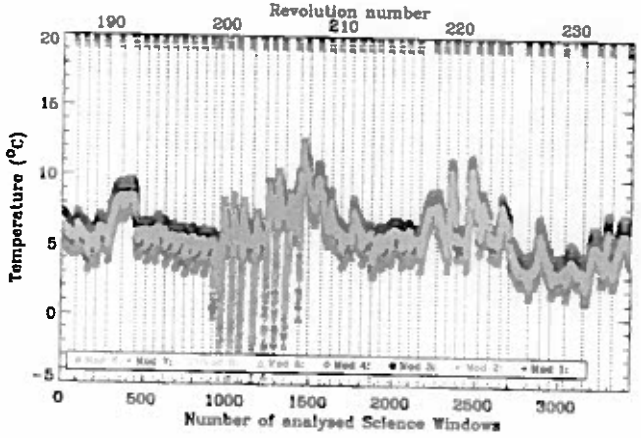

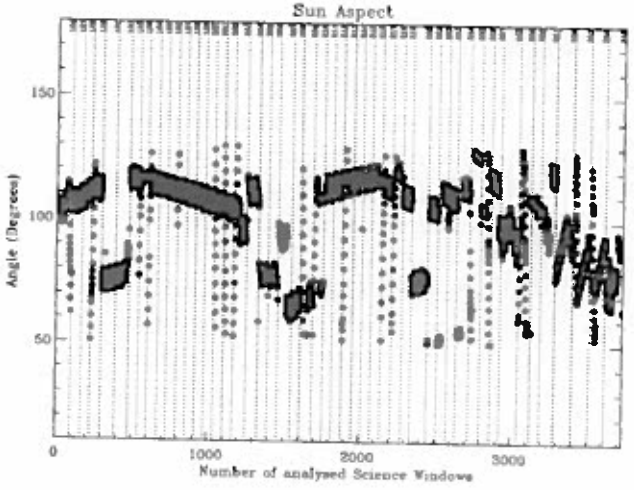

Figure 25: Same as Fig.22 for revolution range 0186 – 0235

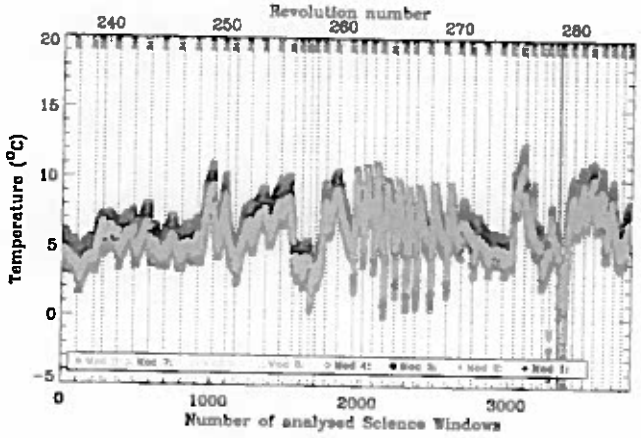

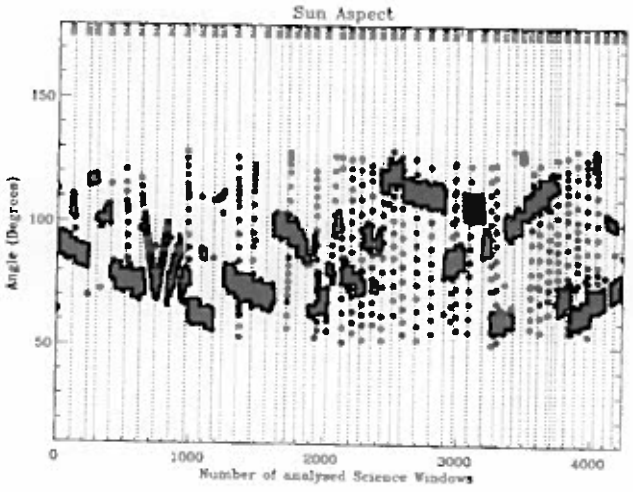

Figure 26: Same as Fig.22 for revolution range 0236 – 0285

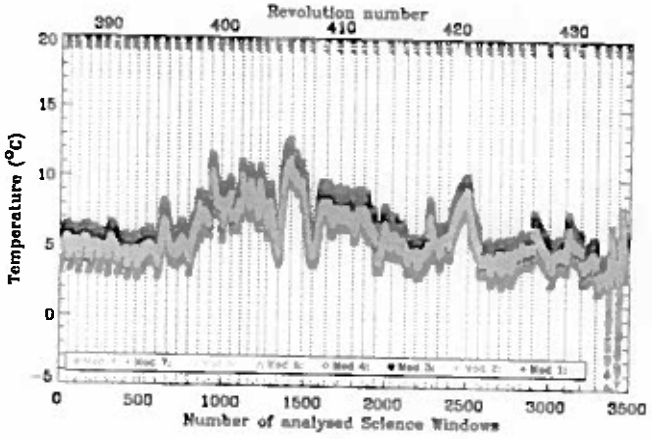

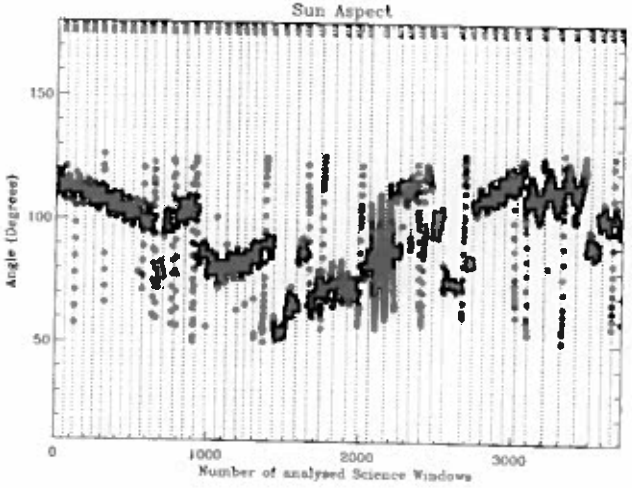

Figure 29: Same as Fig.22 for revolution range 0336 – 0385

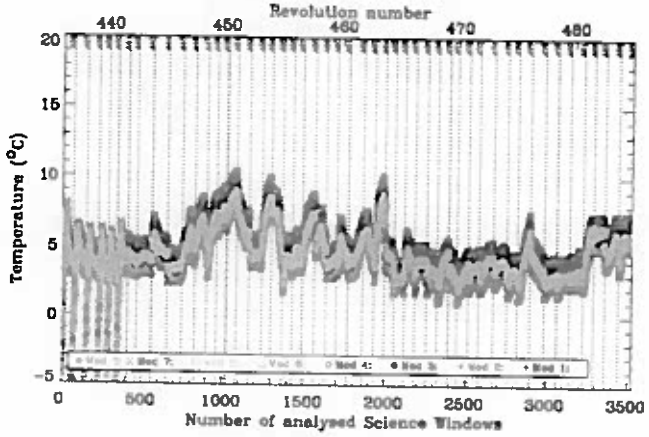

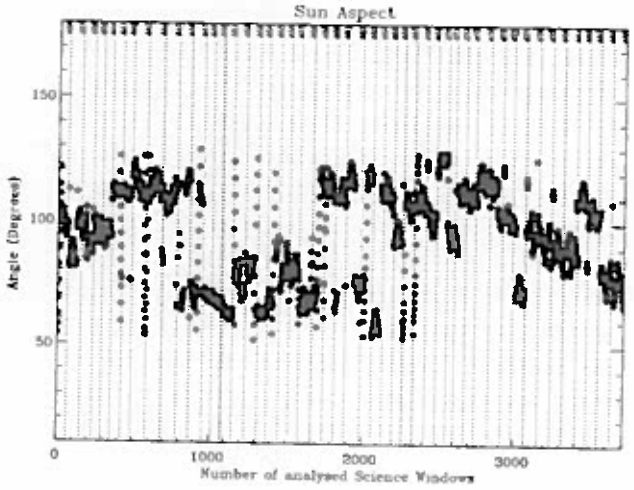

Figure 30: Same as Fig.22 for revolution range 0386 – 0435

10.2 Temperature versus Solar aspect angle

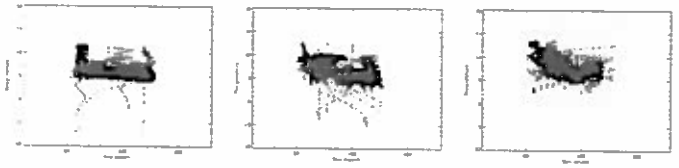

Figure 33: Temperature versus sun aspect angle for each ScW in the revolution range 0036 – 0085 (left panel), 0086 – 0135 (central panel) and 0136 – 0185 (right panel).

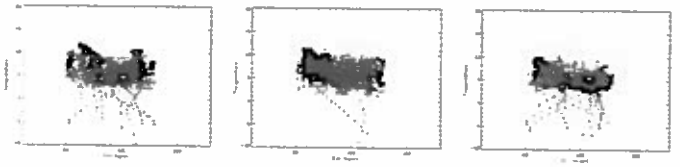

Figure 34: Same as Fig.33 for revolution range 0186 – 0235 (left panel), 0236 – 0285 (central panel) and 0286 – 0335 (right panel).

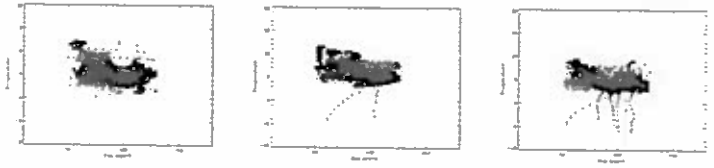

Figure 35: Same as Fig.33 for revolution range 0336 – 0385 (left panel), 0386 – 0435 (central panel) and 0436 – 0485 (right panel).

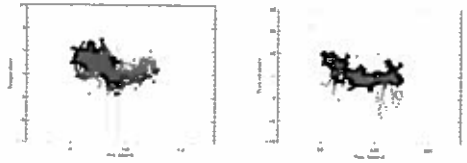

Figure 36: Same as Fig.33 for revolution range 0486 – 0535 (left panel), 0536 – 0585 (central panel) and 0436 – 0485 (right panel).

10.3 Calibration Event Rate

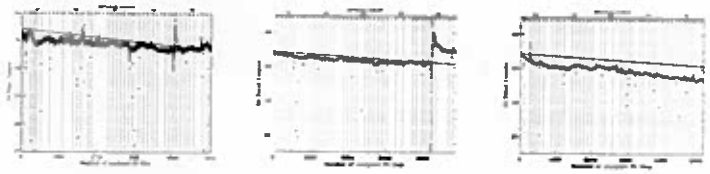

Figure 37: Calibration event rate computed at file level. Left, central and right panel shows respectively revolutions 0036 – 0085, 0086 – 0135 and 0136 – 0185.

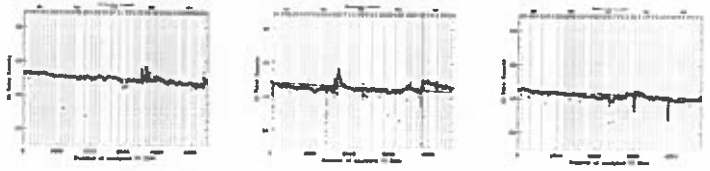

Figure 38: Same as Fig.?? for revolution groups 0186 – 0235, 0236 – 0285 and 0286 – 0335.

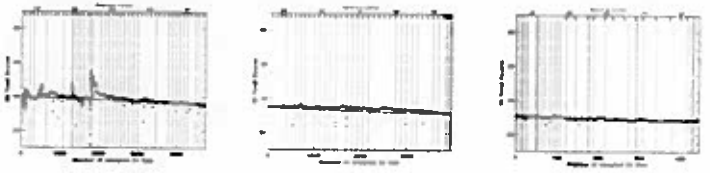

Figure 39: Same as Fig.?? for revolution groups 0336 – 0385, 0386 – 0435 and 0436 – 0485.

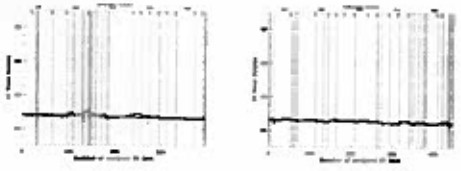

Figure 40: Same as Fig.?? for revolution groups 0486 – 0535 and 0536 – 0585.

10.6 Energy Resolution at 511 keV

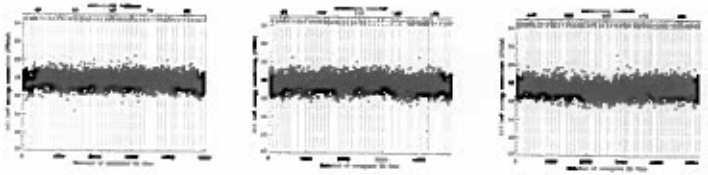

Figure 49: Energy resolution at 511 keV computed at calibration file level, for revolutions 0036 – 0085 (left panel), 0086 – 0135 (central panel) and 0136 – 0185 (right panel).

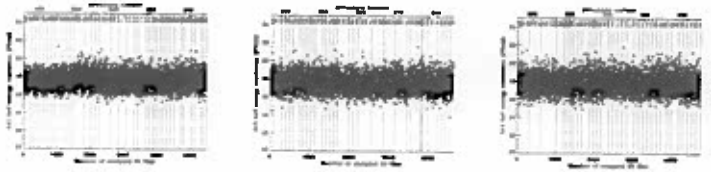

Figure 50: Same as Fig.49 for revolutions 0186 – 0235 (left panel), 0236 – 0285 (central panel) and 0286 – 0335 (right panel).

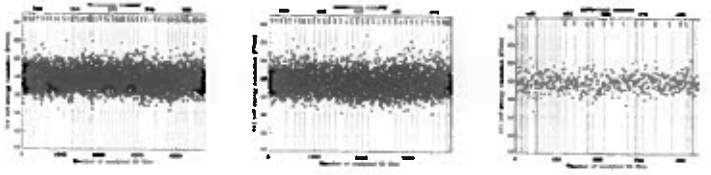

Figure 51: Same as Fig.49 for revolutions 0336 – 0385 (left panel), 0386 – 0435 (central panel) and 0436 – 0485 (right panel).

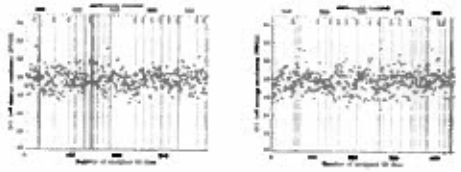

Figure 52: Same as Fig.49 for revolutions 0486 – 0535 (left panel) and 0536 – 0585 (right panel).

10.7 Energy Resolution at 1275 keV

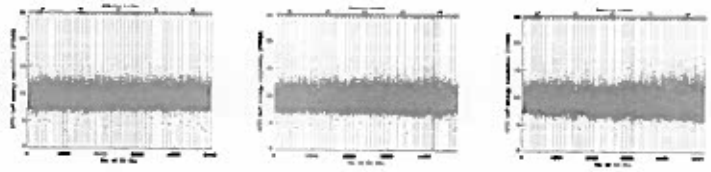

Figure 53: Energy resolution at 1275 keV computed at calibration file level, for revolutions 0036 – 0085 (left panel), 0086 – 0135 (central panel) and 0136 – 0185 (right panel).

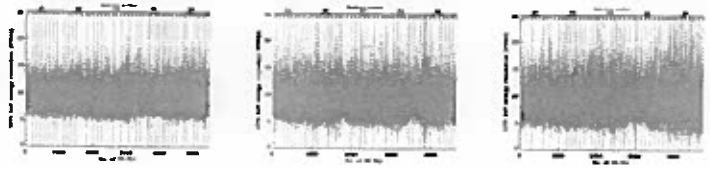

Figure 54: Same as Fig.53 for revolutions 0186 – 0235 (left panel), 0236 – 0285 (central panel) and 0286 – 0335 (right panel).

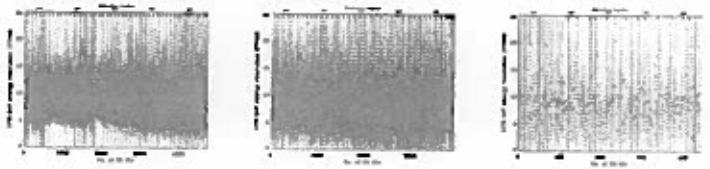

Figure 55: Same as Fig.53 for revolutions 0336 – 0385 (left panel), 0386 – 0435 (central panel) and 0436 – 0485 (right panel).

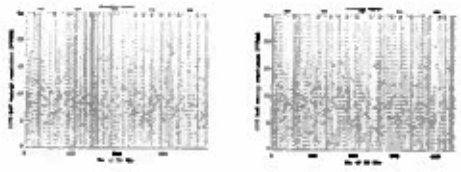

Figure 56: Same as Fig.53 for revolutions 0486 – 0535 (left panel) and 0536 – 0585 (right panel)